Eur. Phys. J. A **31**, 43–51 (2007)
DOI 10.1140/epja/i2005-10318-5

THE EUROPEAN PHYSICAL JOURNAL A

Regular Article – Nuclear Structure and Reactions

A study of pre-equilibrium emission of neutrons in ^{93}Nb(α, xn) reactions

Manoj Kumar Sharma[1,a], H.D. Bhardwaj[2], Unnati[1], Pushpendra P. Singh[1], B.P. Singh[1,b], and R. Prasad[1]

[1] Department of Physics, Aligarh Muslim University, Aligarh (UP)-202 002, India
[2] Department of Physics, DSN College, Unnao (UP)-209 801, India

Received: 20 June 2005 / Revised: 13 October 2006
Published online: 22 January 2007 –
Communicated by C. Signorini

Abstract. With a view to study the pre-equilibrium emission mechanism in α-induced reactions the excitation functions for ^{93}Nb$(\alpha, n)^{96m}$Tc, ^{93}Nb$(\alpha, n)^{96}$Tc, ^{93}Nb$(\alpha, 2n)^{95m}$Tc, ^{93}Nb$(\alpha, 2n)^{95g}$Tc and ^{93}Nb$(\alpha, 3n)^{94}$Tc reactions have been measured in the energy range threshold to ≈ 10 MeV/nucleon using the activation technique. The measured excitation functions have also been compared with theoretical predictions based on the semi-classical code, which takes into account compound nucleus as well as pre-equilibrium emission. The analysis of the data indicates significant contribution from pre-equilibrium emission at these energies particularly in the high-energy tail portion of EFs. The effect of the variation of the parameters used in the code has been studied. The isomeric cross-section ratios have also been measured. It has been observed that the pre-equilibrium fraction increases rapidly with the increase in α-particle bombarding energy.

PACS. 25.55.-e ^{3}H-, ^{3}He-, and ^{4}He-induced reactions – 27.60.+j $90 \leq A \leq 149$

1 Introduction

The availability of medium-energy particle accelerators has made possible the study of charged-particle–induced reactions, which are important in large-scale developments. Applications of measured cross-section data may be found in the nuclear-energy generation and waste management and also in nuclear medicine. The knowledge of cross-sections for neutron emission channels is important in reactor technology, particularly in the recently proposed accelerator driven sub-critical (ADS) reactors, typically known as energy amplifiers. For all these applications, an improved understanding of charged-particle interaction is needed for transport calculations and radiation effects. The charged-particle–induced reactions are also important for the fundamental understanding of the reaction mechanism and to test the validity of various available nuclear-reaction models. The nuclear data required for the above applications come mainly from nuclear scattering and reaction model calculations, which depend on optical models, whose parameters are determined by elastic scattering and the total cross-section data. The measurement and analysis of the EFs is particularly interesting, because the features of the EFs at low, medium and high energies can reveal the reaction mechanism involved. The low-energy portion of EF is dominated by the compound-nucleus (CN) mechanism, however, with increasing the projectile energy, the PE processes become important [1–4]. The high-energy tail portion of the excitation functions (EFs) of the nuclear reactions induced by light-ion medium-energy projectiles has been one of the important signatures of pre-equilibrium (PE) emission. It may, however, be pointed out that considerable data is available in the literature on nucleon– and light-ion–induced reactions but the cross-section values measured by different groups of workers for the same reaction, generally, do not agree. Several authors [3–8] have reported a variety of data for α-induced activation reactions on niobium (Nb) in the energy range from threshold to well above it. Matsuo *et al.* [5] have measured the EFs for (α, n), $(\alpha, 2n)$ and $(\alpha, 3n)$ reactions on ^{93}Nb and have used chemical separation of radioactive residues followed by activity measurement employing the low-resolution NaI(Tl) crystal. In their work Bond and Jha [7] have measured EFs for these reactions employing the solid-state Ge(Li) γ-ray spectrometer. The measurements were mainly carried out [7] with a view to obtain the yield information as a function of energy. Gadioli *et al.* [8], however, have done more detailed measurements and theoretical description has been given in terms of several kinds of reaction mechanism at relatively higher energies in the range $\approx$ 40–140 MeV. As

[a] e-mail: mks_amu@rediffmail.com
[b] e-mail: bpsinghamu@gmail.com

such, their data is above the energy range of interest in the present work. Ernst *et al.* [9] in their paper on "Investigation of α-induced reactions on Niobium and Tantalum" have given the experimentally measured excitation functions for several reactions, however, they have not compared the measured excitation functions with calculated ones using statistical codes. Further, Mukherjee *et al.* [4] have carried out the measurement of isomeric cross-section ratio in the reaction ^{93}Nb$(\alpha, 2n)^{95m+g}$Tc only in the energy range upto 120 MeV with a view to study the PE emission. In order to test the theoretical models, Mukherjee *et al.* [4] have compared the measured EFs with calculations done using various codes [10,11]. It may not be out of place to mention that theoretically it may be possible to reproduce the measured EFs for the prominent reaction channels accurately and separately than trying to describe all open reaction channels simultaneously. It may improve the description of the data for the partial channel at the cost of other open channels, however, it appears unacceptable from the point of view of physics. Several phenomenological as well as quantum-mechanical models have been launched to explain the pre-equilibrium reaction mechanism. These models describe the way in which projectile energy gradually gets redistributed among the constituent nucleons of the composite system through a series of residual two-body interactions. These models have been quite successful in reproducing both the energy spectra of emitted particles and the EFs for the specific product nuclide in a wide range of reactions, but primarily for reactions involving mostly nucleons in the entrance and exit channels in the energy range up to 100 MeV or so. It is interesting to obtain in the analysis, simultaneously, a best description of all existing experimental data for all open channels, as this approach is internally consistent, detailed and complete. Further, the information on the isomeric cross-section ratio of a residual nucleus and its dependence on the incident particle is far from abundant. The study of the isomeric cross-section ratio is of importance from the viewpoint of understanding the reaction mechanism and to test the nuclear models. Several models like ALICE-91 [12], CASCADE [13], PACE2 [14], ACT [15], COMPLETE [10] etc., are available in the literature and are generally used for theoretical calculations of EFs for light- and heavy-ion–induced reactions. In all the codes except ACT [15], the configuration of the codes is such that they predict the total cross-section only for the population of the residual nuclei. However, the code ACT [15] calculates the cross-sections for the production of both the ground as well as isomeric states. As such, in order to obtain theoretical predictions of the population of the isomeric states, in particular, the code ACT [15] based on the lines of codes STAPRE [11] has been used in the present work using consistently the same set of parameters.

In light of the above and with a view to study PE emission in a consistent and systematic way, a programme of precise measurement and analysis of EFs for a large number of α-induced PE-dominated reactions has been undertaken. As a part of this programme, in the present work, EFs for the reactions ^{93}Nb$(\alpha, n)^{96m}$Tc, ^{93}Nb$(\alpha, n)^{96}$Tc, ^{93}Nb$(\alpha, 2n)^{95m}$Tc, ^{93}Nb$(\alpha, 2n)^{95g}$Tc, and ^{93}Nb$(\alpha, 3n)^{94g}$Tc have been measured in the excitation energy range from threshold to $\approx$ 40.8 MeV, using the stacked-foil activation technique and γ-ray spectrometry. One of the applications of technetium isotopes is that it is an excellent corrosion inhibitor for steel. In all these reactions the isotopes of Tc are formed and as such the measured EF may be used for deciding the optimum beam energy for the production of these isotopes. In the present work, the analysis of the measured EFs has been performed within the framework of CN and PE formalisms employing the Hauser-Feshback (HF) [16] and exciton models [17], respectively. The experimental details and errors are given in sect. 2, while, sects. 3 and 4 deal with the results and discussion. The conclusions are given in sect. 5 of the paper.

2 Experimental details

Experiment has been carried out at the Variable Energy Cyclotron Centre (VECC), Kolkata, India, using a collimated α-particle beam of $\approx$ 40 MeV. Self-supporting spectroscopically pure foils of natural niobium have been used as targets. The thickness of these commercially supplied Nb foils was $\approx$ 5 mg/cm^2. The target stack containing 12 Nb samples having aluminium degraders in between them was bombarded by α-particles in the irradiation chamber dedicated to this purpose in *cave one* for about half an hour. A beam current $\approx$ 100 nA was monitored from current integrator count rate. The average beam energy on a given target foil and degrader was calculated using the stopping-power values given in the tables of Northcliffe and Schilling [18]. Post-irradiation analysis has been performed using a high-resolution large-volume (100 c.c.) Ge(Li) detector coupled to a multichannel analyzer CANBERRA-88. The activities induced in various sample foils were recorded using a Ge(Li) detector, which was pre-calibrated using various standard γ-sources. A ^{152}Eu point source was used to determine the efficiency of the detector for different γ-ray energies at various source-detector distances. The sample and detector distances were suitably adjusted so as to minimize the dead time $< 10\%$. Pertinent decay data [19] used in the present work for yield calculations are given in table 1. The residues produced due to different reaction channels were identified by their characteristic γ-rays and measured half-lives. From the observed activities of the residual nuclei, the cross-sections were determined for a given reaction channel using the standard formulation as given below [20]:

$$\sigma_r(E) = \frac{A\lambda \exp(\lambda t_2)}{N_0 \phi \theta K (G\varepsilon)[1-\exp(-\lambda t_1)][1-\exp(-\lambda t_3)]}, \quad (1)$$

where, A is the observed counts (area under the photo peak of the characteristic gamma ray of the particular residues) during the accumulation time t_3 of the induced activity of the decay constant λ, N_0 the number of target nuclei being exposed under the geometrical shadow of the beam irradiated for duration t_1 with a particle beam of

Table 1. List of reactions, identified γ-rays, half-lives and their branching ratios.

Serial No.	Reaction	J^π	Half-life	E_γ (keV)	Branching ratio (%)
1.	^{93}Nb$(\alpha, n)^{96m}$Tc	4^+	51.5 min	1200	1.09
2.	^{93}Nb$(\alpha, n)^{96}$Tc	7^+	4.28 d	778.1	99.79
				812.5	82
				849.9	98
				1126.8	15.20
3.	^{93}Nb$(\alpha, 2n)^{95m}$Tc	1/2	61.0 d	204.0	66.20
4.	^{93}Nb$(\alpha, 2n)^{95g}$Tc	$9/2^{+2}$	20.0 h	765.7	93.00
				947.6	2.14
				1073.3	3.75
5.	^{93}Nb$(\alpha, 3n)^{94g}$Tc	7^+	4.8 h	702.0	99.60
				916.0	7.60

flux ϕ, t_2 the time lapse between the stop of irradiation and the start of counting, θ the branching ratio of the characteristic γ-ray and $G\varepsilon$ the geometry-dependent efficiency of the detector. The factor $[1 - \exp(-\lambda t_1)]$ takes care of the decay of evaporation residue during the irradiation and is typically known as the saturation correction. The correction for the decay of the induced activity due to the delay between the stop of irradiation and the start of counting and during the data accumulation is taken into account via the factors $\exp(\lambda t_2)$ and $[1 - \exp(-\lambda t_3)]$, respectively. $K = [1 - \exp(-\mu d)]/\mu d$ is the correction for the self-absorption of the γ radiation in the sample thickness itself, where d is the thickness of the sample and μ is the γ-ray absorption coefficient.

Various factors which may introduce uncertainties in the present measurements are discussed here. There may be uncertainty in determining the geometry-dependent detector efficiency. The statistical errors of the counting of the standard sources may give rise to the error in efficiency, which was minimized by accumulating large number of the counts for comparatively larger times (≈ 5000 s). Experimental data on the variation of geometry-dependent efficiencies with the γ-ray energy at different source-detector distances has been fitted with the power law curve. The uncertainty due to fitting of the efficiency curve is estimated to be $< 3\%$. Uncertainty in determining the efficiency may also come up due to the solid-angle effect, because the irradiated samples were not point sources like the standard source, but they had a diameter of ≈ 3 mm. It is estimated that the error in the efficiency on account of solid-angle effect is $< 5\%$. The inaccurate estimate of the foil thickness and non-uniformity of foil may give rise to uncertainty in determining the number of target nuclei in the sample. It is estimated from the thickness measurements at different positions of the sample foils that errors due to non-uniform deposition are expected to be $< 1\%$. Errors may come up due to fluctuations in beam current during the irradiation. Although, care was taken to keep the beam current constant within 10%. It is estimated that beam fluctuations may introduce an error of $< 3\%$. During irradiation of the stack, the beam traverses the thickness of the material, thus the initial beam intensity reduces. It is estimated that the error due to decrease in beam intensity is expected to be $< 2\%$. In all these measurements the dead time is kept less than 10% by suitably adjusting the sample-detector distance and the corrections for it were applied in the counting rate. Further, the uncertainties in the branching ratio, decay constant, half-lives etc., which are taken from the table of isotopes have not been taken into account. The overall error due to all these factors is expected to be $< 15\%$ of the measured cross-section values.

3 Results and discussion

The measured excitation functions for the reactions ^{93}Nb$(\alpha, n)^{96m}$Tc, ^{93}Nb$(\alpha, n)^{96}$Tc, ^{93}Nb$(\alpha, 2n)^{95m}$Tc, ^{93}Nb$(\alpha, 2n)^{95g}$Tc, and ^{93}Nb$(\alpha, 3n)^{94g}$Tc have been shown in figs. 1-4 and 6, respectively. In fig. 5, the total cross-section for the Nb$(\alpha, 2n)$ reaction, obtained from the sum of isomeric and ground-state cross-sections, is plotted. The experimental results are presented in table 2 of the paper. The uncertainties reported are the statistical errors of counts and the discrepancies between the independent measurements (different gamma rays) of given nuclei. The horizontal bars in figs. 1-6, represent the beam energy spread obtained from the energy loss in sample thickness. The size of the circle includes the magnitude of statistical errors in cross-section values, if no error bar is plotted. In all the neutron exit channel reactions both the ground state as well as the isomeric states are populated. All the above-mentioned reactions are described separately in the following parts.

3.1 ^{93}Nb(α, n) reaction

The EFs for the reactions ^{93}Nb$(\alpha, n)^{96m}$Tc and ^{93}Nb$(\alpha, n)^{96}$Tc are plotted in figs. 1 and 2, respectively. The isomer ^{96m}Tc produced in the (α, n) reaction decays (98%) to ^{96}Tc via internal transition. The half-life of ^{96}Tc is 4.35 d which is much larger than that of the metastable state ^{96m}Tc ($t_{1/2} = 51.5$ min). As such, the

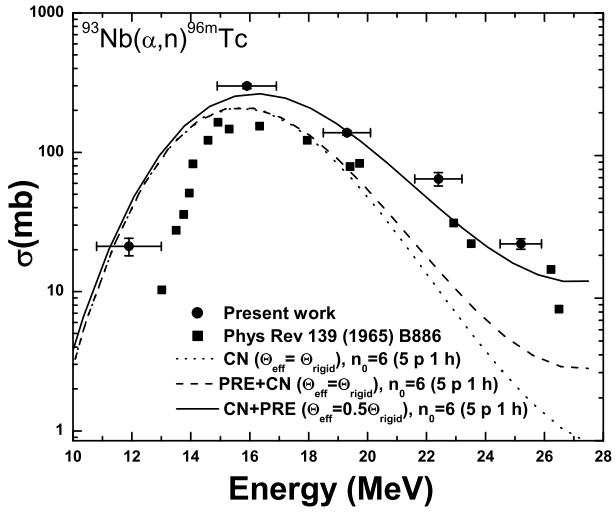

Fig. 1. The experimentally measured and theoretically calculated EFs for the reaction ^{93}Nb$(\alpha, n)^{96m}$Tc. The effect of the variation of the effective momentum of inertia on calculated EFs is also shown.

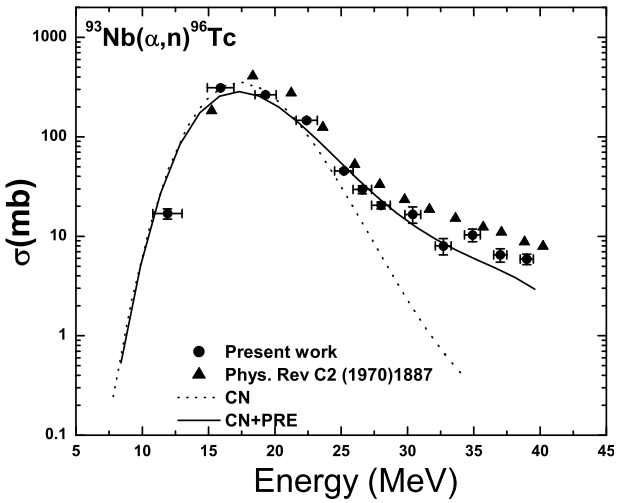

Fig. 2. The experimentally measured and theoretically calculated EFs for the reaction ^{93}Nb$(\alpha, n)^{96}$Tc.

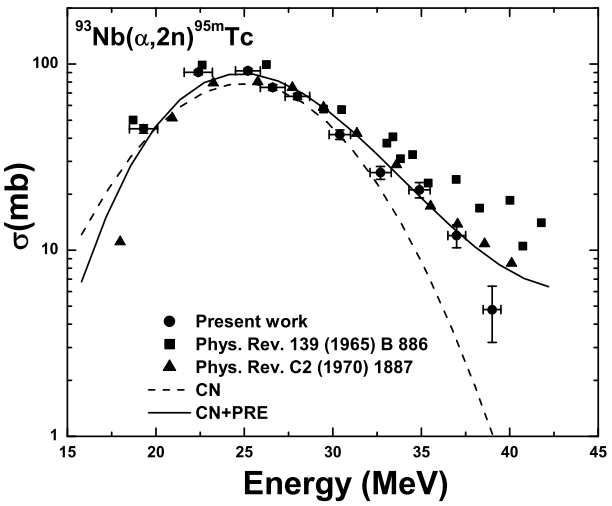

Fig. 3. The experimentally measured and theoretically calculated EFs for the reaction ^{93}Nb$(\alpha, 2n)^{95m}$Tc.

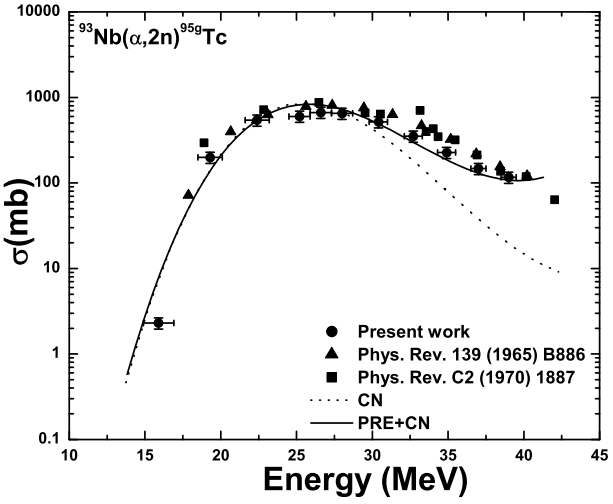

Fig. 4. The experimentally measured and theoretically calculated EFs for ^{93}Nb$(\alpha, 2n)^{95g}$Tc.

observed activity for the residue ^{96}Tc has contribution for both the isomeric and ground-state cross-sections. In fig. 1, the cross-sections for the ^{93}Nb$(\alpha, n)^{96m}$Tc reaction measured by Matsuo *et al.* [5] have also been plotted for comparison. As can be seen from this figure, the measurements of Matsuo *et al.* [5] are lower than the present work in the low-energy region. In fig. 2, presently measured EF for ^{93}Nb$(\alpha, n)^{96}$Tc reaction is shown along with literature data [7]. As can be seen from this figure, the measurements of Bond *et al.* [7] agree with the present work within statistical errors.

3.2 ^{93}Nb$(\alpha, 2n)$ reaction

The EFs for the reactions ^{93}Nb$(\alpha, 2n)^{95m}$Tc and ^{93}Nb$(\alpha, 2n)^{95g}$Tc are given in figs. 3 and 4, respectively. In the ^{93}Nb$(\alpha, 2n)$ reaction, both the ground and metastable states are populated. The metastable state ^{95m}Tc is longer lived with a half-life of 61 d, while the half-life of the ground state ^{95g}Tc is $\approx$ 20 h. The isomeric transition is only 3.9%. The cross-sections for both the states are determined by taking proper account of the isomeric transition. The measurements of Matsuo *et al.* [5] and Bond *et al.* [7] are also presented for both these reactions *i.e.*, ^{93}Nb$(\alpha, 2n)^{95m}$Tc and ^{93}Nb$(\alpha, 2n)^{95g}$Tc and are shown in figs. 3 and 4, respectively. As can be seen from fig. 3, the measurements of Matsuo *et al.* [5] are in general higher than the present work ones, particularly in the tail portion of EF. However, in case of ^{93}Nb$(\alpha, 2n)^{95g}$Tc the literature values agree with the present work. In fig. 5, the excitation function for the reaction ^{93}Nb$(\alpha, 2n)^{95}$Tc, obtained from the sum of cross-sections for isomeric and ground states is shown.

Table 2. Experimentally measured cross-sections.

E_α (MeV)	$\sigma(^{96m}$Tc) (mb)	$\sigma(^{96}$Tc) (mb)	$\sigma(^{95m}$Tc) (mb)	$\sigma(^{95g}$Tc) (mb)	$\sigma(^{95T}$Tc) (mb)	$\sigma(^{94g}$Tc) (mb)
11.9 ± 1.1	21.1 ± 3	16.9 ± 2.0				
15.9 ± 1.0	298.7 ± 11.9	310.8 ± 1		2.3 ± 0.1		
19.3 ± 0.8	138.1 ± 5.3	265.4 ± 2.3	44.9 ± 2.3	199.1 ± 1.5	244 ± 2.7	
22.4 ± 0.8	64.3 ± 7.1	146.1 ± 5.9	90.3 ± 2.6	541.8 ± 0.5	632.1 ± 2.6	
25.2 ± 0.7	22 ± 1.9	45.5 ± 1.9	92.1 ± 2.7	600.15.8	692.1 ± 6.4	
26.6 ± 0.7		29.5 ± 2.7	74.9 ± 2.6	666.6 ± 6.3	741.5 ± 6.8	2.3 ± 0.3
28 ± 0.7		20.5 1.6	67 ± 2.5	651.7 ± 5.8	718.7 ± 6.3	55.9 ± 0.2
30.4 ± 0.6		16.6 ± 3.1	41.8 ± 2.4	516.5 ± 3.7	558.3 ± 4.4	205.7 ± 3.7
32.7 ± 0.6		8 ± 1.5	26.1 ± 2.1	352.1 ± 1.7	378.2 ± 2.7	345.1 ± 1.4
34.9 ± 0.6		10.3 ± 1.5	21.1 ± 2	226.8 ± 1.4	247.9 ± 2.4	483.6 ± 17.8
37 ± 0.5		6.5 ± 1	12 ± 1.7	147.1 ± 0.9	159.1 ± 1.9	477.2 ± 2.9
39 ± 0.5		5.9 ± 0.7	4.8 ± 1.6	116.2 ± 1.0	121 ± 1.9	549.4 ± 2.3

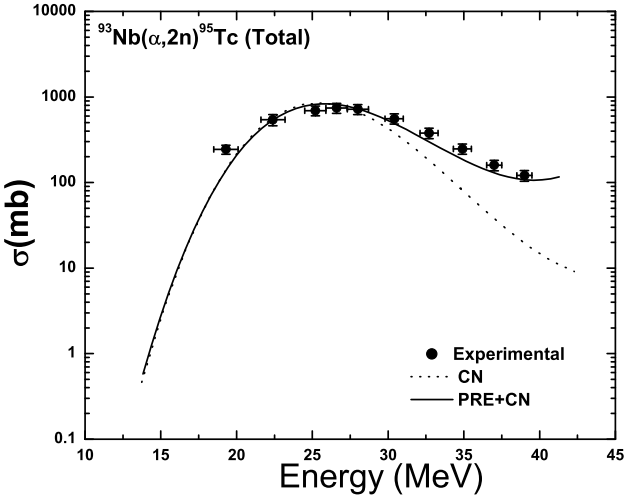

Fig. 5. The experimentally measured total cross-sections (sum of meta + ground states) and theoretically calculated EFs for the reaction ^{93}Nb$(\alpha, 2n)^{95}$Tc.

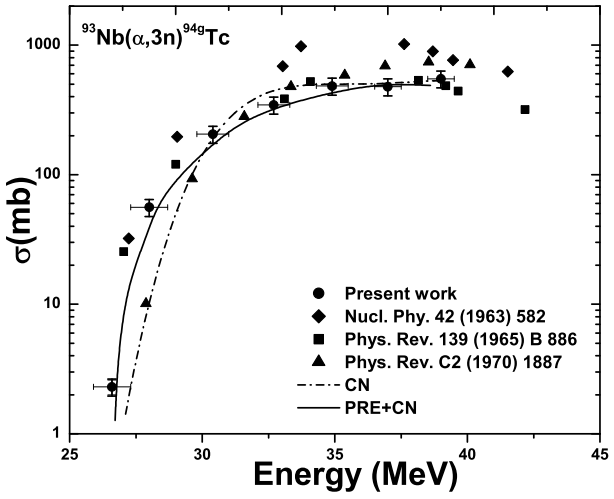

Fig. 6. The experimentally measured and theoretically calculated EFs for the reaction ^{93}Nb$(\alpha, 3n)^{94g}$Tc.

3.3 ^{93}Nb$(\alpha, 3n)$ reaction

In this reaction, both the ground state (^{94g}Tc) as well as the isomeric (^{94m}Tc) states are populated. The decay of these isomers is independent and the half-life of ^{94m}Tc (52.5 min) is smaller than that of the ground state ^{94g}Tc (293 min). The γ-rays of 702, 871 and 916 keV are emitted by the isotope ^{94g}Tc. However, ^{94m}Tc also emits 871 keV γ-rays. These two states of ^{94}Tc decay independently and thus the intensity of the 871 keV γ-ray has contributions due to both these states, hence the separate contribution of the metastable and ground states of ^{94}Tc could not be obtained. The excitation function for the reaction ^{93}Nb$(\alpha, 3n)^{94g}$Tc is shown in fig. 6, along with the literature values. As can be seen from fig. 6, the measurements of Matsuo *et al.* [5] and Bond *et al.* [7] agree to the present measurements in the whole energy range. However, the measurement of Matuszek *et al.* [21] are slightly higher at energies greater than 37 MeV.

Some times the residual nucleus of two different reactions emit γ-rays of nearly the same energy. The γ-ray of 849 keV is emitted in the decay of both the residues ^{96}Tc and ^{94g}Tc produced via ^{93}Nb(α, n) and ^{93}Nb$(\alpha, 3n)$ reactions, respectively. The cross-sections for the ^{93}Nb(α, n) reaction were determined from the observed intensities of the 778 keV, 812 keV and 1126 keV γ-rays coming from ^{96}Tc and the activity of the 849 keV γ-ray was used only up to below the threshold of the ^{93}Nb$(\alpha, 3n)$ reaction. The thresholds for ^{93}Nb$(\alpha, 2n)$ and ^{93}Nb$(\alpha, 2p)$ reactions are very close to each other *i.e.*, $\approx$ 13.1 MeV and $\approx$ 15.5 MeV, respectively. The residual nuclei ^{95m}Tc ($t_{1/2} = 61$ d) and ^{95m}Nb ($t_{1/2} = 3.6$ d) produced by the reactions ^{93}Nb$(\alpha, 2n)^{95m}$Tc and ^{93}Nb$(\alpha, 2p)^{95m}$Nb, respectively, both emit γ-rays of 204 keV. As such, the observed intensity of the 204 keV γ-ray will have contribution from both these reaction channels. Since the absolute intensity of 204 keV γ-rays in ^{95m}Tc is 66.2%, while in ^{95m}Nb it is only 2.34%, as such, the contribution of the $2p$ channel to

the $2n$ channel is expected to be negligibly small. In order to check this, the counting of the samples was performed for several days and the intensity of the 204 keV γ-ray was monitored. The activity of ^{95m}Nb ($t_{1/2} \approx 3.61$ d) was found to drop to the background level after $\approx$ 4–5 half-lives. As such, the remaining activity in the samples was attributed only to the ^{95}Tc and the contribution of the $2p$ channel is negligibly small.

4 Model calculations

Various semi-classical models [17,22–24] are available for theoretical calculations. Quantum-mechanical (QM) theories [25–28], which treat the reaction in terms of statistical multi-step compound (SMC) and statistical multi-step direct (SMD) processes have also been proposed. However, QM theories at present are mostly applicable to the nucleon-induced reactions because for a complex particle in the entrance channel the QM treatment of the initial projectile target interaction becomes very much intricate [29]. In view of the above mentioned fact, the calculations in the present work have been performed employing the semi-classical approach using the code ACT [15].

4.1 Calculations with the code ACT

The theoretical calculations for the excitation functions have been performed using the code ACT [15] which is based on the lines of the code STAPRE [11]. In this code, each evaporation step is treated within the framework of the statistical model with consideration of angular momentum and parity conservation. For the emission of the first particle, PE decay is also taken into the account. The cross-section for the population of both the ground and isomeric states may be calculated using this code. The compound-nucleus calculations are performed using the HF model [16], while the exciton model is employed for the simulation of PE emission. The γ-competition with particle emission is taken into account from the second compound system and onwards. The maximum γ-ray multipolarity of two (dipole) is considered, both for electric and magnetic transitions.

The code ACT [15] first generates a table containing for each CN, the HF denominator $N_i(U, J, \Pi)$ for all excitation energies U in steps of 0.5 MeV bin size and all values of angular momentum J and parity Π, which are required for the subsequent evaporation calculations. These quantities are used for all incident energies for the calculation of excitation functions. The HF denominator is defined as the sum of transmission coefficients for all open channels. The excited state of the residual nucleus is described by the level density $\rho(U, J, \Pi)$. At low excitation energies, the complete information on the quantum numbers of the discrete levels is available. However, in the energy region above the discrete levels, which is referred to as continuum, the level densities are calculated within the framework of the backshifted Fermi gas model by the spin-dependent Lang expression [30]. In this model, it is assumed that the levels with positive and negative parities have the same density. Some of the important parameters of the code are the level density parameter a, the effective moment of inertia Θ_{eff}, and the backshift Δ. In the present calculations, the level density was calculated from the backshifted formula and the level density parameters given in ref. [31] are used. In the cases when the level density parameters a are not known, they were selected for the calculation by interpolating the data of the neighboring isotopes, taking into account the odd-even systematics [31,32]. In some cases the level density parameters were required to be varied within 20% in order to get a better description of the data. As a typical example, the effect of variation of the level density parameters a on calculated EFs is discussed elsewhere [33]. In the present work, a value of $a = 13.07$ of the first compound nucleus ^{97}Tc gives a satisfactorily representation of the experimental data, however, its interpolation value was 11.37 [31]. This variation of the level density parameters is justified, since these parameters are empirical in nature and are valid [31] in the energy range up to 20 MeV only. Further, any change in the effective value of the moment of inertia (Θ_{eff}), and the temperature (T) of the nucleus may influence the spin cut-off parameter (σ) given by the expression [32]

$$\sigma^2 = \Theta_{eff} \frac{T}{\hbar^2}. \tag{2}$$

In the present calculations, the effective moment of inertia Θ_{eff}, has been taken equal to the rigid-body value (Θ_{rig}), assuming the nucleus to be as a solid sphere, *i.e.*

$$\Theta_{rig} = \frac{2}{5} mA(r_0 A^{1/3})^2, \tag{3}$$

where, $r_0 = 1.25$ fm, A is the mass number and m the nucleon mass. The transmission coefficients required in the calculations are generated by a code TLK, which uses the global optical model potentials [34]. The transmission coefficients are assumed to depend on the orbital angular momentum and on the energy of the relative motion only. The separation energies needed in these calculations are taken from the tables of Wapstra and Bos [35], and the decay scheme of various nuclei from the table of isotopes [19].

The equilibration of the compound system is treated within the framework of the exciton model [17]. Starting from a simple configuration, the composite system is assumed to equilibrate through a series of two-body interactions and may emit particles from all intermediate stages. The states of the system are classified according to the number of excitons or more specifically to the numbers n_p and n_h of the excited particle and hole degrees of freedom, respectively. The application of a two-body interaction to the state of a (n_p, n_h) configuration leads to states with $(n_p + 1, n_h + 1)$, (n_p, n_h) or $(n_p - 1, n_h - 1)$ excited particles and holes. In competition with these internal transitions, particles can be emitted from each stage. For all these processes transition rates averaged over all states of a configuration are calculated. These transition rates λ_+, λ_0 and λ_- are related by the Williams expression [36],

corrected for Pauli principle by Cline [37] to $|\bar{M}|^2$, the absolute value of the square of the average effective matrix element for two-body residual interactions:

$$\lambda_+ = \frac{2\pi}{\hbar}|\bar{M}|^2\frac{g^3}{U^2}(n+1), \quad (4)$$

$$\lambda_0 = \frac{2\pi}{\hbar}|\bar{M}|^2 g n_p n_h (n-2), \quad (5)$$

$$\lambda_- = \frac{2\pi}{\hbar}|\bar{M}|^2 g^2 U\frac{(3n-2)}{4}. \quad (6)$$

In order to evaluate internal transition rates, it is necessary to calculate $|\bar{M}|^2$. However, at present no microscopic calculations for $|\bar{M}|^2$ are available [38]. As such, the expression $|\bar{M}|^2 = F_M \cdot A^{-3}U^{-1}$ proposed by Kalbach-Cline [39], where A is the mass number and U the excitation energy of composite system, is used for calculating the value of the matrix element. Here, F_M is a constant and is treated as an adjustable parameter to match the experimental data. In the literature, values of F_M ranging from 95–7000 MeV^3 are proposed [28,40] for reproducing the experimental data. The average rates for the emission of particle are calculated from the principle of detailed balance considerations. The single-particle state density g, used in the transition rate calculations, is obtained from the level density parameter a using the relation $g = 6\pi^{-2}a$.

For PE decay the initial number n_0 of excited particles and holes and the parameter F_M, which is given by equation $|\bar{M}|^2 = F_M \cdot A^{-3}U^{-1}$ and defines the matrix for internal transition rates, are required to be given in the first input data and may be treated as parameters of the model. In the literature, the values of the initial exciton number n_0 ranging from 4 to 6 are used for α-induced reactions. In some of our earlier analysis [15,41, 42] of excitation functions for α-induced reactions on several targets (A = 55, 59, 63, 65, 121, 128, 130, 165, 197 and 209) where measurements were done to cover the tails of the excitation functions, a value of $n_0 = 6$ along with $F_M = 430$ MeV^3 was found to give a satisfactory reproduction of the experimental data. In the present analysis also, the same value of the initial exciton number $n_0 = 6$ ($n_p = 5$, $n_h = 1$) and $F_M = 430$ MeV^3 has been retained and found to give a satisfactory reproduction of the excitation functions, in general, for all the reactions studied presently as shown in figs. 1-6. In all these calculations the value of the effective moment of inertia Θ_{eff} has been taken equal to the rigid-body value, *i.e.* Θ_{rig}. The experimentally measured EFs agree well with these calculations, in general, except for the reaction ^{93}Nb$(\alpha, n)^{96m}$Tc. The calculations for this reaction were again performed with the $\Theta_{eff} = 0.5\Theta_{rig}$ value and it is found that there is surprisingly a good agreement between calculation and experimental data. The same is again reflected in the isomeric cross-section ratio, as discussed in sect. 4.2.

The configuration of the 6-exciton state may be justified [15,41,42] as the first interaction may give rise to the excitation of one particle above the Fermi energy leaving behind a hole in the excited state, *i.e.* in all 5 particles and one hole. The amount of PE emission depends on how successfully particle decay competes with internal transition and, therefore, is determined by the respective rates and the initial exciton number. Figure 7 displays the influence of variation of F_M (*i.e.*, of internal transition rates) and the initial exciton number n_0 on the calculated excitation function for the ^{93}Nb$(\alpha, n)^{96}$Tc reaction. It may be observed from fig. 7 that a lower value of the exciton number gives, in general, higher pre-equilibrium contributions. This is evident as a smaller value of n_0 means larger number of two-body interactions prior to the establishment of equilibrium characteristic of compound nucleus resulting in the large pre-equilibrium contribution. Further, a lower value of F_M means a smaller value of $|\bar{M}|^2$ and hence lower internal transition rates. Consequently, continuum decay rates for a given value of n_0 will be relatively enhanced resulting in a large pre-equilibrium contribution. In the present work, the calculations have been performed using first only the compound-nucleus model and it has been observed that the high-energy tail portion of excitation functions was underestimated, as shown in fig. 2. However, when the PE contribution is added to these calculations with $n_0 = 6$ and $F_M = 430$ MeV^3, in general, a satisfactory reproduction of the experimental data for the presently measured excitation functions has been obtained. As such, it may be mentioned that there is significant contribution from PE emission for these channels at higher energies.

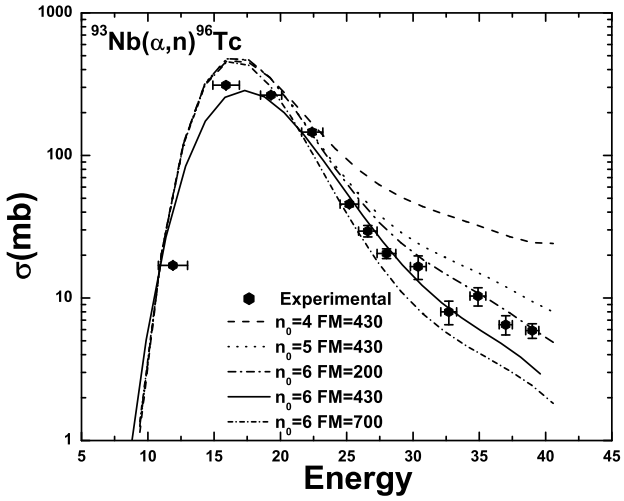

Fig. 7. The experimentally measured and theoretically calculated EFs for the reaction ^{93}Nb$(\alpha, n)^{96}$Tc. The effect of the variation of parameters n_0 and F_M on calculated EFs is also shown.

4.2 Isomeric cross-sections ratio

Isomeric states of a given nucleus have relatively long half-lives, they slightly differ in their energies and have large difference in their spins. Some nuclear reactions populate both the isomeric and the ground states. The ratio of the population of these states is generally called "isomeric cross-section ratio". Since the model used in the

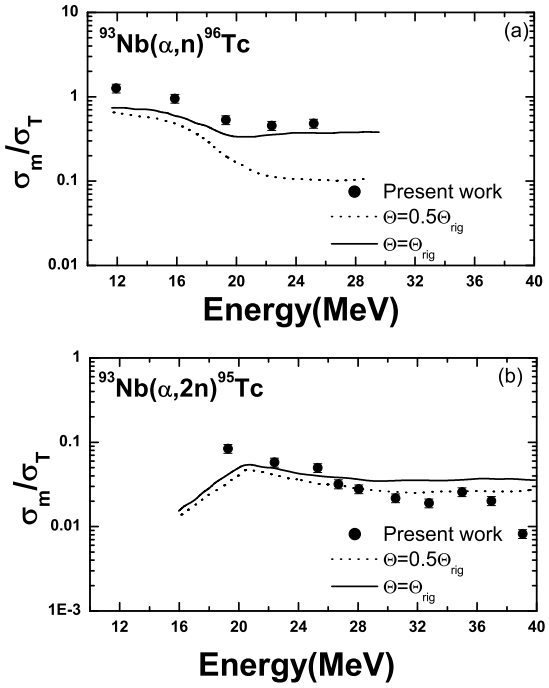

Fig. 8. The experimentally measured and theoretically calculated isomeric cross-section ratios for the reactions ^{93}Nb$(\alpha, n)^{96}$Tc and ^{93}Nb$(\alpha, 2n)^{95}$Tc. The effect of the variation of the moment of inertia on calculated isomeric ratios is also shown.

present work gives a satisfactory representation of the experimental data, it may be considered that the assumptions used in the code ACT [29] are correct. If the ratio σ_m/σ_T, *i.e.* the ratio of the high-spin product to the low-spin product in an (α, xn) reaction is plotted, it should invariably increase with bombarding energy as higher l-waves are admitted and average spin $\langle J_c \rangle$ of the compound nucleus increases. The isomeric ratio in residual nuclei from nuclear evaporation processes cannot increase indefinitly because of the effect of competing reactions. It is possible to calculate the EFs for both the ground as well as isomeric states separately using the code ACT [29]. In all the presently studied reactions both these states are populated. In the following discussion, the isomeric cross-section ratio is defined as the ratio of the cross-section for the population of the isomeric state σ_m to the total cross-section σ_T for the population of both isomers $\sigma_T = \sigma_m + \sigma_g$. The study of the isomeric cross-section ratio (σ_m/σ_T) may give information on the angular-momentum effects in nuclear reactions. The experimental isomeric cross-section ratios σ_m/σ_T for the reactions ^{93}Nb(α, n) and ^{93}Nb$(\alpha, 2n)$ are determined at different α-particle bombarding energies and are shown in fig. 8(a-b). Since higher partial waves participate in reactions with higher bombarding energy, the isomeric cross-section ratio is expected to be a function of the incident projectile energy. The spins of the isomeric states ^{96m}Tc $(J = 4^+)$ and ^{95m}Tc $(J = 1/2^-)$ are lower than the respective ground-state spins ^{96}Tc $(J = 7^+)$ and ^{95g}Tc $(J = 9/2^+)$. It is known that the PE particles carry away the significant

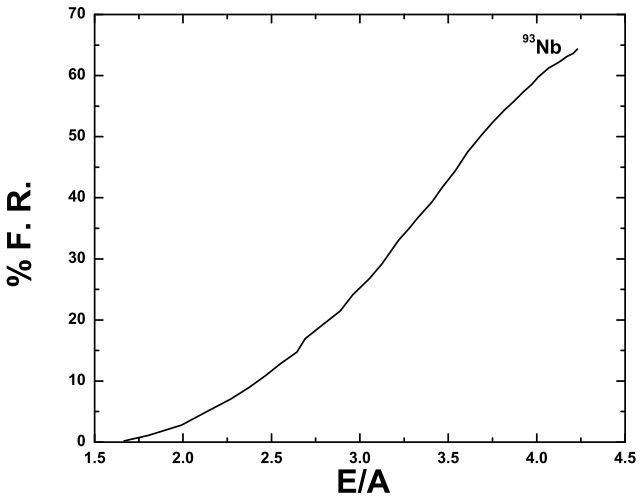

Fig. 9. Pre-equilibrium fraction as a function of excitation energy per nucleon.

amount of angular momentum from the compound system, hence, the isomeric cross-section ratio is expected to depend strongly on the initial spin distribution of the CN. The isomeric cross-section ratio initially decreases with the increase in α-particle bombarding energy and soon levels off. It may be due to the fact that, with further increase in excitation energy, more channels open up, as a result, larger angular momentum will be carried away by the ejectiles and hence the ratio does not increase above a certain energy. Thus the isomeric ratio becomes nearly constant. The isomeric ratios in ^{96}Tc and ^{95}Tc are observed to become nearly constant above α-energies of ≈ 20 and ≈ 30 MeV, respectively. In fig. 8(a-b), the experimental isomeric cross-section ratios are also compared with the ones calculated theoretically with two options of the moment of inertia using the code ACT. In the first option the effective moment of inertia Θ_{eff} is taken equal to the rigid-body value, while in the second option the effective moment of the inertia $\Theta_{eff} = 0.5\Theta_{rig}$ is taken. It may be observed from fig. 8, that the experimental isomeric cross-section ratios for the reactions ^{93}Nb$(\alpha, n)^{96m}$Tc and ^{93}Nb$(\alpha, n)^{96}$Tc are better reproduced when the calculations are performed with the effective moment of inertia equal to the rigid-body value, however the theoretical isomeric cross-section ratios are close to the experimental ones for the reactions ^{93}Nb$(\alpha, 2n)^{95m}$Tc and ^{93}Nb$(\alpha, 2n)^{95g}$Tc, when $\Theta_{eff} = 0.5\Theta_{rig}$ is taken. The effective moment of inertia at low excitation energies is expected to be less than to the rigid-body value and should approach towards the rigid-body value with increase in excitation energy [43].

4.3 Pre-equilibrium fraction

The total pre-equilibrium fraction "FR", which is a measure of the relative strength of the PE component needed to reproduce the experimental EFs has also been calculated [3]. FR reflects the relative importance of equilibrium and PE processes. The total FR at a given excitation

energy may be defined as the ratio of the sum of the cross-sections for PE emission of all emitted particles (restricted to n, p, d and α) to the total cross-section. The PE fraction for the target ^{93}Nb is calculated and is shown in fig. 9. As can be seen from this figure, the pre-equilibrium fraction increases rapidly with the increase in α-particle bombarding energy per nucleon, which indicates the dominance of PE emission at relatively higher energies.

5 Conclusions

The excitation functions and the isomeric cross-section ratios for α-induced reactions in ^{93}Nb are presented in the energy range threshold to ≈ 40 MeV. It may be concluded that the high-energy tails of the EFs of α-induced reactions cannot be accounted for by the pure compound-nucleus mechanism and they have contributions from the PE emission. The proper admixture of EQ and PE processes is needed for a better reproduction of the experimentally measured excitation functions. An attempt has been made to fix the two important free parameters of the exciton model and a value of $n_0 = 6$ along with $F_M = 430\,\mathrm{MeV}^3$ is found to give the best fit to the experimental data. The pre-equilibrium fraction has been found to be energy dependent.

The authors are thankful to the Chairman, Department of Physics, A.M.U. Aligarh for extending the necessary facilities. Further, we would like to acknowledge the VECC personnel for all its help during the experiments. One of the authors (MKS) thanks the Department of Science and Technology (DST), New Delhi, India, for providing financial support vide the project no. SR/FTP/PS-46/2003.

References

1. M. Blann, Ann. Nucl. Sci. **25**, 123 (1975).
2. J. Pal, C.C. Dey, P. Banerjee, S. Bose, B.K. Sinha, M.B. Chatterjee, Phys. Rev. C **71**, 03605 (2005).
3. B.P. Singh, Manoj K. Sharma, M.M. Muthafa, H.D. Bhardwaj, R. Prasad, Nucl. Instrum. Methods Phys. Res. A **562**, 717 (2006).
4. S. Mukherjee, N.L. Singh, G. Kiran Kumar, L. Chaturvedi, Phys. Rev. C **72**, 014609 (2005).
5. T. Matsuo, J.M. Matuszek jr., N.D. Dudey, T.T. Sugihara, Phys. Rev. B **139**, 886 (1965).
6. C.L. Branquihno, S.M.A. Hoffmann, G.W.A. Newton, V.J. Robinson, H.Y. Wang, I.S. Grant, J. Inorg. Nucl. Chem. **41**, 617 (1970).
7. P. Bond, S. Jha, Phys. Rev. C **2**, 1887 (1974).
8. E. Gadioli, E. Gadiolli-Ebra, J.J. Hogan, B.V. Jacab, Phys. Rev. C **29**, 76 (1984).
9. J. Ernst, W. Friedland, H. Stockhorst, Z. Phys. A **308**, 301 (1982).
10. J. Ernst, W. Friedland, H. Stockhorst, Z. Phys. A **328**, 333 (1987).
11. M. Uhl, B. Strohmair, Report IRK 76/01 (1981) NEA Data Bank (Cedex) France.
12. M. Blann, NEA Data Bank, Gif-sur-Yvette, France, Report PSR-146 (1991).
13. F. Puhlhofer, Nucl. Phys. A **280**, 267 (1977).
14. A. Garvon, Phys. Rev. C **21**, 230 (1980).
15. H.D. Bhardwaj, PhD Thesis, A.M.U. Aligarh, India (1985).
16. W. Hauser, H. Feshbach, Phys. Rev. **87**, 366 (1952).
17. J.J. Griffin, Phys. Rev. Lett. **17**, 478 (1966)
18. L.C. Northcliffe, R.F. Schilling, Nucl. Data Tables A **7**, 256 (1970).
19. C.M. Lederer, V.S. Shirley, *Table of Isotopes VII* (John Wiley, New York, 1978).
20. N.L. Singh *et al.*, Can. J. Phys. **67**, 870 (1989).
21. J.M. Matuszek jr., T.T. Sugihara, Nucl. Phys. **42**, 582 (1963).
22. R. Serber, Phys. Rev. **72**, 1114 (1947).
23. M. Blann, Phys. Rev. Lett. **27**, 337 (1971).
24. M. Blann, Phys. Rev. Lett. **28**, 757 (1972).
25. H. Feshbach, A. Kerman, S. Koonin, Ann. Phys. **125**, 429 (1980).
26. Klaus Debertin, Richard G. Helmer *Gamma-and X-Ray spectrometry with semiconductor detector* (Elsevier Science Publisher B.V., Amsterdam, 1988).
27. D. Agassi, H.A. Weidenmuller, G. Mantzouranis, Phys. Rep. **22**, 145 (1975).
28. T. Udagawa, K.S. Low, T. Tamura, Phys. Rev. C **28**, 1033 (1983).
29. H. Gruppelaar, P. Nagel, P.E. Hodgson, Riv. Nuovo. Cimento **9**, No. 1 (1986).
30. D.W. Lang, Nucl. Phys. **77**, 545 (1966).
31. W. Dilg, W. Schantl, H. Vonach, Nucl. Phys. A **217**, 269 (1973).
32. S. Sudar, S.M. Qaim, Phys. Rev. C **73**, 034613 (2006).
33. B.P. Singh, H.D. Bhardwaj, R. Prasad, Can. J. Phys. **69**, 1376 (1991).
34. M. Blann, H.K. Vonach, Phys. Rev. C **28**, 1475 (1983).
35. A.H. Wapstra, K. Bos, At. Data Nucl. Data Tables **19**, 215 (1977).
36. F.C. Williams jr., Phys. Rev. Lett. B **31**, 184 (1970).
37. C.K. Cline, Nucl. Phys. A **186**, 273 (1972).
38. H. Jahn, *Nuclear Theory for Applications*, IAEA-SMR 93 report (1982) p. 39.
39. C. Kalbach-Cline, Nucl. Phys. A **210**, 590 (1973).
40. K.K. Gudima, S.G. Mashnik, V.D. Toneev, Nucl. Phys. A **401**, 329 (1983).
41. B.P. Singh, M.G.V. Sankaracharyulu, M. Afzal Ansari, H.D. Bhardwaj, R. Prasad, Phys. Rev. C **47**, 2055 (1993).
42. B.P. Singh, PhD Thesis, Aligarh Muslim University, India (1992).
43. N.D. Dudey, T.T. Sugihara, Phys. Rev. B **139**, 886 (1969).